Mon. Not. R. Astron. Soc. **375,** 1059–1069 (2007) doi:10.1111/j.1365-2966.2006.11375.x

An extreme rotation measure in the high-redshift radio galaxy PKS B0529–549⋆

J. W. Broderick,[1]† C. De Breuck,[2] R. W. Hunstead[1] and N. Seymour[3]

[1]*School of Physics, University of Sydney, Sydney, NSW 2006, Australia*
[2]*European Southern Observatory, Karl Schwarzschild Straße 2, D-85748 Garching, Germany*
[3]*Spitzer Science Center, California Institute of Technology, Mail Code 220-6, 1200 East California Boulevard, Pasadena, CA 91125, USA*

Accepted 2006 December 5. Received 2006 December 1; in original form 2006 October 6

ABSTRACT

We present the results of a radio polarimetric study of the high-redshift radio galaxy PKS B0529−549 ($z = 2.575$), based on high-resolution 12-mm and 3-cm images obtained with the Australia Telescope Compact Array. The source is found to have a rest-frame Faraday rotation measure of -9600 rad m^{-2}, the largest seen thus far in the environment of a $z > 2$ radio galaxy. In addition, the rest-frame Faraday dispersion in the screen responsible for the rotation is calculated to be 5800 rad m^{-2}, implying rotation measures as large as $-15\,400$ rad m^{-2}. Using supporting near-infrared (near-IR) imaging from the Very Large Telescope, we suggest that the rotation measure originates in the Lyα halo surrounding the host galaxy, and estimate the magnetic field strength to be $\sim$10 μG. We also present a new optical spectrum of PKS B0529−549 obtained with the New Technology Telescope, and propose that the emission-line ratios are best described by a photoionization model. Furthermore, the host galaxy is found to exhibit both hot dust emission at 8.0 μm and significant internal visual extinction ($\sim$1.6 mag), as inferred from *Spitzer Space Telescope* near/mid-IR imaging.

Key words: polarization – galaxies: active – galaxies: high-redshift – galaxies: individual: PKS B0529−549 – radio continuum: galaxies.

1 INTRODUCTION

As inferred from the Hubble K–z diagram (e.g. Eales et al. 1997; van Breugel et al. 1998; Jarvis et al. 2001; De Breuck et al. 2002; Inskip et al. 2002; Willott et al. 2003; Rocca-Volmerange et al. 2004), high-redshift radio galaxies (HzRGs; $z > 2$) are among the most-massive galaxies in the early Universe, and are thus crucial in enhancing our knowledge of galaxy formation and evolution. Of particular interest are the environments in which these systems reside. HzRGs are frequently located in regions of overdensity where companion galaxies are often aligned with the axis of radio emission (e.g. Röttgering et al. 1996; Pentericci et al. 2001; Bornancini, Lambas & De Breuck 2006), are potentially members of proto-clusters (e.g. Kurk et al. 2000; Pentericci et al. 2000b; Venemans et al. 2002), and are immersed in huge quantities of gas, as inferred from the extended emission of Lyα (up to $\sim$150 kpc in extent, e.g. Reuland et al. 2003; Villar-Martín et al. 2003, 2006) and CO (e.g. De Breuck et al. 2003; Greve, Ivison & Papadopoulos 2004; Klamer et al. 2005).

In the radio domain, a powerful tool that can be used to investigate the environments of HzRGs is polarimetry. As a linearly polarized wave propagates through a magnetized plasma, the plane of polarization is subject to rotation. The amount by which the plane of polarization rotates is described by the Faraday rotation measure (RM, measured in rad m^{-2}):

$$\mathrm{RM} = 812 \int_0^L n_\mathrm{e} \boldsymbol{B} \cdot \mathrm{d}\boldsymbol{l}, \tag{1}$$

where L is the path length in kpc, n_e is the thermal electron density in cm^{-3}, and $\boldsymbol{B}$ is the magnetic field strength in μG. The integral is taken along the line of sight. It is generally believed that the Faraday screen causing the rotation is located in the vicinity of the radio source. If we assume that the magnetic fields do not vary substantially from galaxy to galaxy, then the RM is an effective indicator of the ambient density of a radio source.

High-resolution multifrequency studies with the Very Large Array (VLA) have discovered a number of HzRGs with significantly high intrinsic RMs. Carilli, Owen & Harris (1994) observed RMs in excess of 1000 rad m^{-2} in the HzRGs B2 0902+343 ($z = 3.395$) and 4C 41.17 ($z = 3.800$). Subsequent investigations of samples of HzRGs with $z \gtrsim 2$ (Carilli et al. 1997; Athreya et al. 1998;

⋆Based on observations collected at the European Southern Observatory (ESO), La Silla, Chile (programme 077.A-0471), and on observations made with the European Southern Observatory telescopes obtained from the ESO/ST-ECF Science Archive Facility (programme 64.P-0500).

†E-mail: jess@physics.usyd.edu.au

Pentericci et al. 2000a) discovered that 20–30 per cent of the sources have RMs in excess of 1000 rad m^{-2}, up to a maximum of 6250 rad m^{-2} in the $z = 2.156$ radio galaxy PKS B1138−262. Such extreme RMs suggest that these HzRGs are situated in very dense environments, analogous to cluster observations at low redshift (Carilli & Taylor 2002, and references therein). Moreover, Pentericci et al. (2000a) have shown that the fraction of powerful radio galaxies with large Faraday rotation significantly increases with increasing redshift; this is consistent with the highest-redshift sources, on average, residing in the densest environments.

In this paper, we present a study of the polarimetric properties of the HzRG PKS B0529−549 ($z = 2.575$), based on high-resolution 12-mm and 3-cm polarimetric observations obtained with the Australia Telescope Compact Array (ATCA). In Section 2, we summarize the previous observations of PKS B0529−549. In Section 3, we describe our ATCA radio data, as well as supporting optical spectroscopy and near/mid-infrared (near/mid-IR) imaging obtained with the ESO New Technology Telescope (NTT), the ESO Very Large Telescope (VLT), and the *Spitzer Space Telescope*. We analyse our radio and optical/IR observations in Sections 4 and 5, before discussing both the polarimetric and host galaxy properties in Section 6. Finally, we present our conclusions in Section 7.

Throughout this paper, we assume a flat Λ cold dark matter cosmology with $H_0 = 71$ km s^{-1} Mpc^{-1}, $\Omega_{\rm M} = 0.27$ and $\Omega_\Lambda = 0.73$ (Spergel et al. 2003). In this cosmology, 1 arcsec = 8.14 kpc at $z = 2.575$. We also define the radio spectral index α by the relation $S_\nu \propto \nu^\alpha$, where S_ν is the flux density at frequency ν.

2 PREVIOUS OBSERVATIONS

PKS B0529−549 was originally selected as part of an unpublished ATCA study of southern HzRG candidates by Wieringa, Hunstead & Liang (private communication). The source was chosen using the ultrasteep spectrum (USS) selection technique (Blumenthal & Miley 1979; Tielens, Miley & Willis 1979), which has been very successful in identifying HzRGs. The two-point spectral index selection criteria were $\alpha_{408}^{2700} < -1.1$ and $\alpha_{2700}^{5000} < -1.0$, where the 408-MHz flux density was taken from the Molonglo Reference Catalogue (MRC; Large et al. 1981), and the 2700- and 5000-MHz flux densities from the old Parkes Catalogue (PKS; Bolton, Savage & Wright 1979, and references therein). PKS B0529−549 was included in the Leiden compendium of USS sources and was found to have a spectroscopic redshift $z = 2.575$ (Röttgering et al. 1997).

Table 1 contains the radio flux densities of PKS B0529−549 measured in previous observations and from this paper. For each measurement, we list the observing frequency, the flux density, its associated uncertainty, and the survey or telescope from which the flux density was obtained. The 4800- and 8640-MHz data points are from the unpublished Wieringa, Hunstead & Liang (private communication) study. At 4800 MHz, the source is slightly extended, while at 8640 MHz, it is a clear Fanaroff–Riley type II (FR II) double.

3 CURRENT OBSERVATIONS AND DATA REDUCTION

3.1 ATCA

We observed PKS B0529−549 with the ATCA on UT 2006 March 31. A full 12-h synthesis was conducted in the 12-mm band with the 6C array configuration, spanning baselines from 153 to 6000 m. Observations were carried out simultaneously at frequencies of 16 448 and 18 496 MHz with bandwidths of 128 MHz. The primary calibrator was PKS B1934−638, while phase calibration was performed in cycles of 2 min every 15 min using PKS B0537−441. We also used PKS B0537−441 as our pointing calibrator, updating the antenna pointing models at intervals of ∼1 h. From imaging PKS B0537−441, we estimate the positional accuracy of the 16 448- and 18 496-MHz images to be ∼0.1 arcsec; the position of PKS B0537−441 itself is known to ∼0.6 mas from very long baseline interferometry measurements (Beasley et al. 2002). The total integration time spent on the target was ∼8 h.

Data reduction followed standard procedures in MIRIAD (Sault, Teuben & Wright 1995). The sensitivity was optimized by using natural weighting to construct total intensity (Stokes *I*) dirty images, which were CLEANed for a total of 500 iterations. To remove the effects of CLEAN bias, we restricted the CLEAN to a box placed around the source. The dynamic range was then improved by applying self-calibration to the CLEANed images. First, one iteration of phase self-calibration was performed, followed by another four iterations of both amplitude and phase self-calibration. The resultant images were primary beam-corrected. The synthesized beamwidth is 1.07×0.75 arcsec^2 at 16 448 MHz (position angle 4.°2) and 0.94×0.66 arcsec^2 at 18 496 MHz (position angle 4.°9), while the rms noise level is 75 μJy beam^{-1} at 16 448 MHz and 110 μJy beam^{-1} at 18 496 MHz.

Table 1. PKS B0529−549 radio flux densities.

Frequency (MHz)	S_ν (mJy)	σ (mJy)	Survey/Telescope	Reference
(1)	(2)	(3)	(4)	(5)
408	2710	350	MRC	Large et al. (1981)
843	1220	37	SUMSS	Mauch et al. (2003)
2700	300	22	PKS	Bolton, Savage & Wright (1977)
4800	158	8	ATCA	Wieringa, Hunstead & Liang (private communication)
4850	142	11	PMN	Wright et al. (1994)
5000	150	21	PKS	Bolton, Savage & Wright (1977)
8640	72	4	ATCA	Wieringa, Hunstead & Liang (private communication)
16 448	33.9	1.4	ATCA	This paper
18 496	29.7	1.6	ATCA	This paper

Notes. Column (1): observing frequency, measured in MHz, column (2): flux density, measured in mJy, column (3): flux density uncertainty, measured in mJy, column (4): survey or telescope from which the flux density was obtained; MRC – Molonglo Reference Catalogue, SUMSS – Sydney University Molonglo Sky Survey, PKS – Parkes Catalogue, ATCA – Australia Telescope Compact Array, PMN – Parkes–MIT–NRAO Survey, and column (5): reference for flux density measurement.

To study the radio properties of PKS B0529−549 in greater detail, we combined our 12-mm data with the 8640-MHz ATCA observations from the Wieringa, Hunstead & Liang (private communication) study.[1] Snapshot-mode observations were carried out on UT 1993 January 6 with the 6A array, spanning baselines from 337 to 5939 m, and a 128-MHz bandwidth correlator configuration. The total integration time was ∼50 min, consisting of five cuts of ∼10 min duration. We re-analysed this data set using PKS B1934−638 as the primary calibrator and PKS B0522−611 as the secondary calibrator. Uniform weighting was necessary to resolve the two lobes. We used the same CLEANing and self-calibration strategy as described above to produce a CLEANed Stokes I image. The synthesized beamwidth is 2.08×0.68 arcsec^2 (position angle $7\overset{\circ}{.}8$), while the rms noise level is 315 μJy beam^{-1}.

To enable a polarimetric analysis of PKS B0529−549, we produced Stokes Q and U images from the self-calibrated visibilities at each of the three available frequencies. All dirty images were lightly CLEANed for a maximum of 50 iterations. The MIRIAD task IMPOL was then used to make total polarized intensity images [flux density $S_P = (S_Q^2 + S_U^2)^{1/2}$] that were corrected for Ricean bias. The rms noise level in the Q and U images, σ_{QU}, is 300, 65 and 90 μJy beam^{-1} at 8640, 16 448 and 18 496 MHz, respectively.

3.2 NTT

The discovery spectrum of PKS B0529−549 (Röttgering et al. 1997) shows bright Lyα at $z = 2.575$ and very weak lines of C IV λ1549, He II λ1640 and C III] λ1909. To confirm these lines, determine their spatial extent and their relative strengths, we obtained a new spectrum on UT 2006 July 28 using the ESO Multi-Mode Instrument (EMMI; Dekker, Delabre & Dodorico 1986) on the NTT. Conditions were non-photometric with ∼1.1 arcsec seeing. We used grism no. 2 and a 1.5 arcsec slit. The target was acquired into the slit by blind offsetting from a nearby (∼25 arcsec) star. To minimize the effects of differential atmospheric refraction, we placed the slit at the parallactic angle. The parallactic angle itself (84°) was close to the radio axis position angle (104°; see Section 4.4). The observations consisted of 3×30 min exposures. After each exposure, we shifted the target by 10 arcsec along the slit to remove the fringing in the red part of the CCD. The dispersion was 3.5 Å pixel^{-1}, the spectral resolution was 14 Å full width at half-maximum (FWHM) and the pixel size was 0.33 arcsec.

We used standard procedures in IRAF to reduce the spectrum. First, we performed bias and flat-field corrections, before removing cosmic rays with the IRAF task SZAP. We then used the IRAF task BACKGROUND to perform the sky subtraction. The resultant frames were median-combined and the 1D spectrum was extracted using a 2 arcsec aperture width, which was chosen to optimize the signal-to-noise ratio (S/N) in the extended emission lines. The spectrophotometric standard EG 274 (Hamuy et al. 1992, 1994) was used for the flux calibration, and an He–Ar arc lamp was used for the wavelength calibration. We estimate the relative flux calibration to be accurate to ∼5 per cent, the absolute flux calibration to within a factor of 2, and the wavelength calibration to ∼0.15 Å, that is, ∼1 per cent of the spectral resolution. Last, the spectrum was corrected for Galactic extinction using both the Schlegel, Finkbeiner & Davis (1998) dust maps [colour excess $E(B - V) = 0.066$ mag] and the Cardelli, Clayton & Mathis (1989) extinction law.

[1] These data were downloaded from the Australia Telescope Online Archive (http://atoa.atnf.csiro.au).

3.3 VLT

We obtained H- and K_s-band images of PKS B0529−549 from the ESO science archive.[2] The observations took place on UT 1999 November 27 and 28 with the Infrared Spectrometer and Array Camera (ISAAC; Moorwood et al. 1998) on the Antu unit (UT1) of the VLT. In both cases, the total integration time was 10 min, consisting of a 10-point jitter pattern of 60-s exposures. The pixel size is 0.147 arcsec in both images and the seeing was ∼0.4 arcsec in H and ∼0.7 arcsec in K_s. We reduced the data using the GASGANO package and calibrated the photometry and astrometry using the Two-Micron All-Sky Survey (2MASS; Skrutskie et al. 2006) catalogue. We estimate the photometry to be accurate to ∼0.1 mag and the relative astrometry to ∼0.2 arcsec.

3.4 *Spitzer*

Spitzer near/mid-IR images of PKS B0529−549 were obtained from the *Spitzer* survey of high-redshift radio galaxies (Seymour et al., in preparation). The observations were carried out on UT 2004 November 26 with the Infrared Array Camera (IRAC; Fazio et al. 2004). The images are at wavelengths of 3.6, 4.5, 5.8 and 8.0 μm and consist of 4×30 s exposures. Details concerning the data reduction are given in Seymour et al. (in preparation). We used 2MASS to calibrate the astrometry, which we estimate to be accurate to ∼0.2 arcsec.

4 ANALYSIS OF RADIO PROPERTIES

Table 2 contains a number of radio properties of PKS B0529−549 determined from this study. In particular, for each source component, we list its J2000 position, integrated flux density, fractional polarization, spectral index and rotation measure. These properties are discussed in the following sections.

4.1 Morphology

Fig. 1 shows the radio morphology of PKS B0529−549 at 8640, 16 448 and 18 496 MHz. At all three frequencies, the source has an FR II double morphology. It is clear that the lobes are asymmetric: the eastern lobe is approximately three to four times brighter than the western lobe. The lobe separation is ∼1.2 arcsec at all three frequencies, corresponding to a projected linear size of ∼10 kpc in our adopted cosmology. Thus, PKS B0529−549 is a compact steep-spectrum (CSS) source (see e.g. the review by O'Dea 1998).

4.2 Flux densities and spectral indices

Peak and integrated flux densities were measured by fitting elliptical Gaussians to both source components with the MIRIAD task IMFIT. The fitting errors were calculated following Condon (1997) and combined in quadrature with the calibration uncertainty to obtain a total flux density uncertainty. In general, the fitting uncertainty is much smaller than the calibration uncertainty, which is ∼5 per cent at 8640 and 16 448 MHz and ∼6.5 per cent at 18 496 MHz. The total 8640-MHz flux density calculated from our re-analysis is consistent with the value determined by Wieringa, Hunstead & Liang (private communication).

[2] http://archive.eso.org.

Table 2. PKS B0529−549 radio properties derived from ATCA observations.

Component	RA (J2000)	Dec. (J2000)	8640 MHz		16 448 MHz		18 496 MHz		α	RM
	(h m s)	(° ′ ″)	S_I (mJy)	m (per cent)	S_I (mJy)	m (per cent)	S_I (mJy)	m (per cent)		(rad m^{-2})
(1)	(2)		(3)		(4)		(5)		(6)	(7)
East	05 30 25.53	−54 54 23.5	55.2 ± 2.8	4.7 ± 0.6	26.3 ± 1.3	7.8 ± 0.3	23.4 ± 1.5	8.4 ± 0.4	−1.14 ± 0.09	−720 ± 80
West	05 30 25.39	−54 54 23.2	20.7 ± 1.1	<5.3	7.6 ± 0.4	4.9 ± 1.2	6.3 ± 0.4	7.6 ± 1.9	−1.56 ± 0.10	...

Notes. Column (1): source component, column (2): position of source component in J2000 coordinates, columns (3)–(5): integrated Stokes I flux density, S_I, measured in mJy, and fractional linear polarization, m, expressed as a percentage (3σ upper limit at 8640 MHz), at 8640, 16 448 and 18 496 MHz, column (6): spectral index of source component, and column (7): observed-frame rotation measure, not corrected for the Galactic Faraday screen, measured in rad m^{-2}.

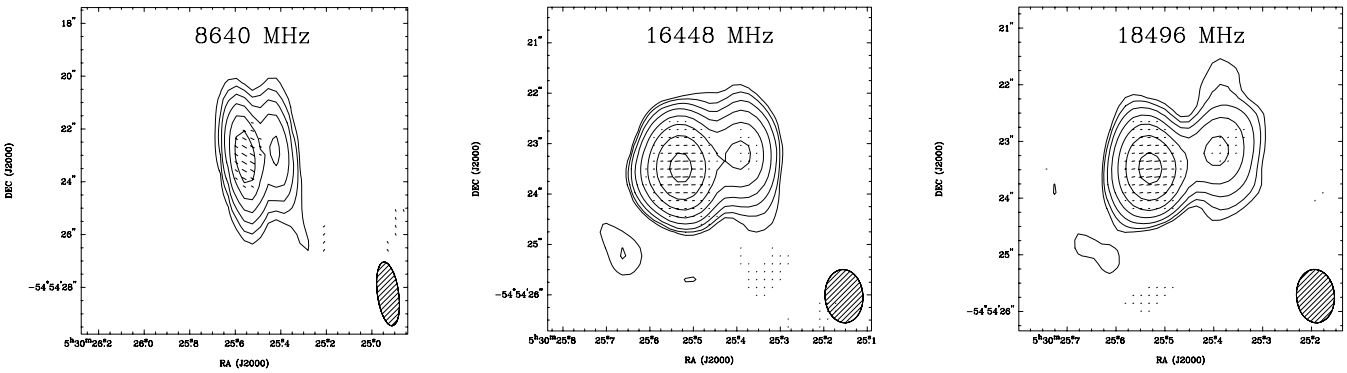

Figure 1. PKS B0529−549 radio contour plots at 8640, 16 448 and 18 496 MHz with ***E*** polarization vectors superposed. In the left-hand panel, the contour levels are 1, 2, 4, 8, 16 and 32 mJy beam^{-1}. In the middle panel, the contour levels are 0.15, 0.3, 0.6, 1.2, 2.4, 4.8, 9.6 and 19.2 mJy beam^{-1}. In the right-hand panel, the contour levels are 0.25, 0.5, 1, 2, 4, 8 and 16 mJy beam^{-1}. The synthesized beam is shown in the bottom right-hand corner of each panel.

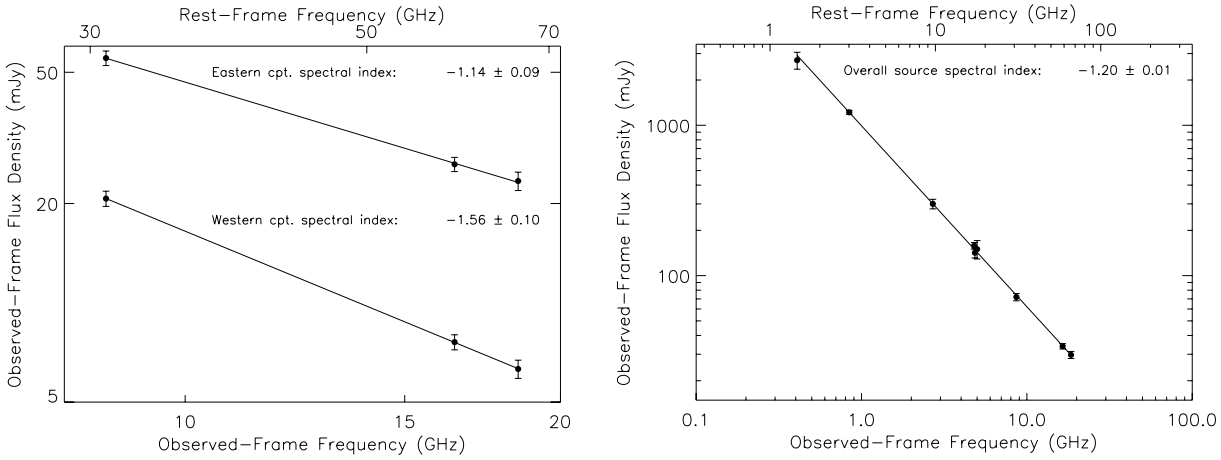

Figure 2. Radio SEDs of the eastern and western components of PKS B0529−549 (left-hand panel) and the overall source (right-hand panel). In each panel, the axes are labelled in both observed- and rest-frame frequencies. Spectral indices derived from linear least-squares fits with inverse-variance weighting are stated next to each SED.

The spectral energy distributions (SEDs) of the individual source components and the overall source are shown in Fig. 2. For each source component, we calculated three-point spectral indices using the 8640-, 16 448- and 18 496-MHz flux densities. We also derived an overall source spectral index using the flux density information in Table 1 combined with our 8640-, 16 448- and 18 496-MHz flux densities. As is evident in Fig. 2, each spectrum can be fitted by a single power law. The western lobe has a much steeper spectral index ($\alpha = -1.56$) than the eastern lobe ($\alpha = -1.14$). The overall spectral index is $\alpha = -1.20$. Using this value, the radio luminosity at 1.4 GHz is calculated to be 4.7×10^{28} W Hz^{-1}.

4.3 Fractional polarization

The fractional linear polarization m is given by

$$m = \frac{\sqrt{S_Q^2 + S_U^2}}{S_I}, \tag{2}$$

with uncertainty

$$\sigma_m \approx \frac{\sigma_{QU}}{S_I}. \tag{3}$$

We only considered pixels with polarized intensity $>3\sigma_{QU}$ when calculating m. We do not detect any linearly polarized flux at the

3σ level at 8640 MHz in the western lobe. Moreover, the linearly polarized flux in the western lobe is only detected at the 4σ level at 16 448 and 18 496 MHz. The lack of sensitivity in the fractional polarization measurements in the western lobe meant that we could not use the Laing–Garrington effect (Garrington et al. 1988; Laing 1988) to deduce the relative orientation of the lobes to the line of sight.

As the ATCA has a multichannel continuum mode, one can minimize the effects of bandwidth depolarization by dividing each bandpass of effective bandwidth 104 MHz into 13 channels of bandwidth 8 MHz. However, we found that the average fractional polarization values obtained from this approach did not differ significantly from those obtained using the full bandwidth. This is expected, given that bandwidth depolarization becomes progressively less important with increasing frequency (e.g. Gardner & Whiteoak 1966).

It is interesting to compare the fractional polarization measurements in PKS B0529−549 with those obtained in other high-frequency studies. The median 8.2-GHz fractional polarization of the hotspots in the CSS sources from the Carilli et al. (1997) and Pentericci et al. (2000a) studies is 4.5 per cent, which is consistent with the 8.6-GHz fractional polarization in the eastern lobe of PKS B0529−549. Moreover, given that these CSS sources are at similar redshifts to PKS B0529−549 (median redshift ∼2.5), the agreement is also valid at rest-frame frequencies. Similarly, in both the observed and the rest frames, the 8.6-GHz fractional polarization in the eastern lobe is consistent with the median 8.5-GHz fractional polarization of 4.6 per cent observed in source components in the B3–VLA CSS sample (Fanti et al. 2004) in the redshift range 2–3 (median redshift ∼2.3).

The 16.5- and 18.5-GHz fractional polarization values in the eastern and western lobes of PKS B0529−549 are comparable with the Ricci et al. (2004) ATCA study of southern Kühr sources ($S_{5\,\mathrm{GHz}} \geqslant 1$ Jy); the median fractional polarization at 18.5 GHz for steep-spectrum radio galaxies in their sample is 6.1 per cent. However, in the ATCA 20-GHz pilot survey, Sadler et al. (2006) found a median fractional polarization of only 2.3 per cent in a flux-limited sample with $S_{20\,\mathrm{GHz}} \geqslant 100$ mJy, though there is a trend for fainter 20-GHz sources to show higher levels of fractional polarization. Given that the 16.5- and 18.5-GHz flux densities of PKS B0529−549 are approximately one-third of this limiting flux density, our results are consistent with the Sadler et al. (2006) study. We note that in both the Ricci et al. and Sadler et al. samples there is not enough redshift information to permit an investigation at rest-frame frequencies.

4.4 Rotation measure

The rotation measure RM is determined from the linear relationship between polarization position angle (Φ) and observing wavelength squared (λ^2):

$$\Phi = \Phi_0 + (\mathrm{RM})\lambda^2, \tag{4}$$

where Φ_0 is the intrinsic polarization position angle. The polarization position angle, measured from the north to the east, was found using

$$\Phi = \frac{1}{2}\tan^{-1}\left(\frac{S_U}{S_Q}\right), \tag{5}$$

with uncertainty

$$\sigma_\Phi \approx \frac{\sigma_{QU}}{2S_P}. \tag{6}$$

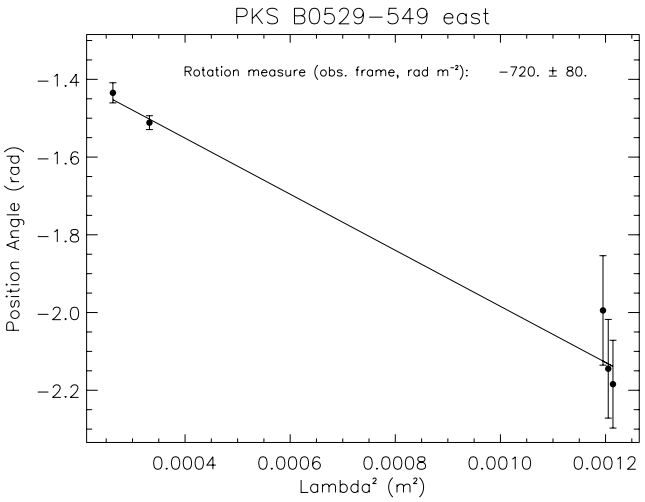

Figure 3. Polarization position angle versus λ^2 for the eastern lobe of PKS B0529−549. The observed-frame RM (not corrected for the Galactic Faraday screen), derived from a least-squares linear fit with inverse-variance weighting, is stated in the upper right-hand corner of the panel.

We used the values of Φ calculated at the position of peak intensity to determine the RM. The Φ vectors at each frequency are shown in Fig. 1.

We only had sufficient S/N to derive an RM for the stronger, eastern radio component. The non-detection of linear polarization at 8640 MHz in the western lobe limits our λ^2 baseline to two closely spaced points. The length of this baseline, coupled with the fact that linear polarization is only detected at the 4σ level at 16 448 and 18 496 MHz meant that the precision in the RM measurement was low.

Fig. 3 shows a plot of Φ versus λ^2 and the corresponding linear fit for the eastern lobe of PKS B0529−549. We found that the $n\pi$ ambiguity in Φ was best solved by dividing the 8640-MHz bandpass into three approximately equally-spaced bins (centres 8676, 8644 and 8608 MHz) and subtracting π rad from the measured position angles at these frequencies. It is clear in Fig. 3 that the data are well fitted by a linear relation (reduced $\chi^2 = 0.58$). The observed-frame RM is -720 ± 80 rad m^{-2}.

If the Faraday screen producing the RM is located at the redshift z of the source, then the intrinsic RM, $\mathrm{RM_{intr}}$, is related to the observed RM, $\mathrm{RM_{obs}}$, such that

$$\mathrm{RM_{intr}} = (\mathrm{RM_{obs}} - \mathrm{RM_{gal}}) \times (1+z)^2, \tag{7}$$

where $\mathrm{RM_{gal}}$ is the contribution to the RM from the Galactic Faraday screen. As there are very few published extragalactic RMs in the vicinity of PKS B0529−549, interpolating $\mathrm{RM_{gal}}$ to the position of PKS B0529−549 (Galactic coordinates $l = 262\overset{\circ}{.}7$, $b = -33\overset{\circ}{.}4$) may introduce considerable uncertainties. Therefore, to determine $\mathrm{RM_{gal}}$, we used the median RM of sources no more than 15° from PKS B0529−549 from the all-sky RM catalogue of Broten, MacLeod & Vallee (1988). $\mathrm{RM_{gal}}$ was found to be 30 rad m^{-2}, which is consistent with the foreground Galactic RM in the direction of the Large Magellanic Cloud (Gaensler et al. 2005), ∼15° from PKS B0529−549. Thus, given that the redshift of PKS B0529−549 is $z = 2.575$, then $\mathrm{RM_{intr}} = -9600 \pm 1000$ rad m^{-2}.

After correcting for Faraday rotation, the intrinsic position angle of the magnetic field in the eastern lobe at the position of peak intensity is $18° \pm 2°$. The position angle of the radio axis is $-76° \pm 2°$. Therefore, the magnetic field is oriented at ∼90° to the jet

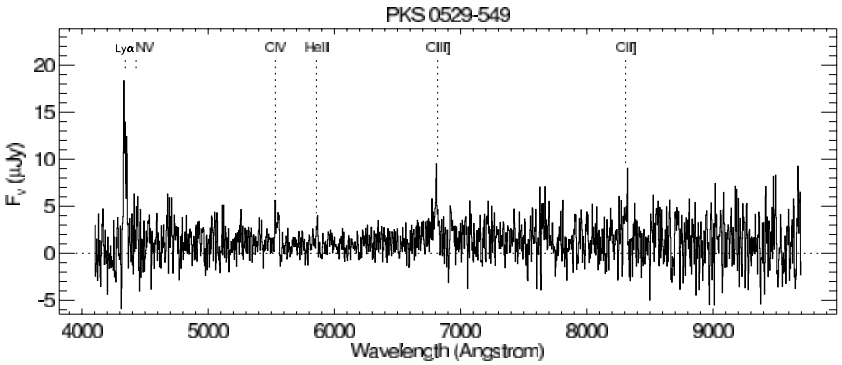

Figure 4. NTT EMMI spectrum of PKS B0529−549. Prominent emission-line features have been marked. The positions of the vertical dotted lines indicate the predicted observed wavelength of the lines at the redshift quoted in Table 3.

direction in the lobe hotspot, which is typically observed in powerful radio galaxies (e.g. Muxlow & Garrington 1991). Moreover, using minimum energy conditions (Miley 1980), we estimate the magnetic field strengths in the eastern and western lobe hotspots to be ∼450 and ∼750 μG, respectively. In comparison, the hotspot magnetic field strengths in the Carilli et al. (1997) and Pentericci et al. (2000a) studies span the range 160–700 μG.

5 ANALYSIS OF OPTICAL/INFRARED DATA

5.1 NTT spectroscopy

In this section, we discuss the properties of PKS B0529−549 derived from our NTT spectrum, which is shown in Fig. 4. Our spectrum has a higher S/N than the Röttgering et al. (1997) spectrum, allowing us to clearly detect Lyα, C IV λ1549, He II λ1640 and C III] λ1909, as well as marginal N V λ1240 and C II] λ2326. Using these emission lines, our redshift determination ($z = 2.570 \pm 0.005$) agrees with the redshift calculated in the Röttgering et al. (1997) study ($z = 2.575 \pm 0.002$), within the limits of experimental uncertainty. The emission-line properties deduced from the spectrum are listed in Table 3. For each detected emission line, we give the observed line wavelength, integrated flux density, deconvolved FWHM and rest-frame equivalent width.

The main difference between our spectrum and the one presented in Röttgering et al. (1997) is that we find the C IV flux to be ∼2.5 times stronger and the C III] flux to be approximately two times weaker, such that line ratio C IV/C III] ≈ 1.0. We note that our 2-arcsec extraction aperture is smaller than the one used in the Röttgering et al. (1997) study, who chose an aperture as large as the angular extent of Lyα, which they calculated to be 5 arcsec. This means that our 1D spectrum will be missing some of the extended flux in the emission lines.

Using the NTT 2D spectrum of PKS B0529−549, we find the angular size between the most extreme points where Lyα is detected to be 5.1 arcsec, in good agreement with the value calculated by Röttgering et al. (1997). Our value is also comparable to the Lyα extent between the spatial points where the emission-line flux is 20 per cent of the peak level, as calculated by van Ojik et al. (1997) from a higher-resolution (∼3 Å) spectrum of the Lyα emission. In our adopted cosmology, this angular size of 5.3 arcsec implies that PKS B0529−549 is surrounded by a Lyα halo of spatial extent ∼45 kpc.

Using the information in Table 3, and considering only those emission lines with clear detections, we derive line ratios C IV/He II ≈ 2.8, C III]/He II ≈ 2.7, C IV/C III] ≈ 1.0, C IV/Lyα ≈ 0.16 and C III]/Lyα ≈ 0.15. We note that any absorption or resonant scattering effects will tend to decrease the Lyα flux, and so the C IV/Lyα and C III]/Lyα line ratios should be viewed as upper limits. By plotting these ratios in line diagnostic diagrams, we can determine the excitation mechanism (photoionization or shock ionization) that best describes the data (Allen, Dopita & Tsvetanov 1998; De Breuck et al. 2000b). Our improved measurements suggest that the line ratios are most consistent with a photoionization model with power-law index of the ionizing spectrum $\alpha = -1.0$ and ionization parameter $\log(U) \sim -2$. This result is in agreement with previous studies of the high-excitation line ratios in HzRGs, where it was found that photoionization models provide the best fit to the data

Table 3. PKS B0529−549 emission-line measurements.

z	Line	$\lambda_{\rm obs}$ (Å)	Integrated flux (10^{-16} erg s^{-1} cm^{-2})	$\Delta v_{\rm FWHM}$ (km s^{-1})	$W_\lambda^{\rm rest}$ (Å)
(1)	(2)	(3)	(4)	(5)	(6)
2.570 ± 0.005	Lyα	4340 ± 2	6.3 ± 0.7	1860 ± 380	>275
	N V λ1240[a]	4436 ± 5	0.76 ± 0.24	900 ± 800	>17
	C IV λ1549	5542 ± 11	1.0 ± 0.1	1810 ± 830	17 ± 5
	He II λ1640	5863 ± 3	0.36 ± 0.07	400 ± 290	11 ± 4
	C III] λ1909	6807 ± 3	0.97 ± 0.14	1060 ± 310	31 ± 6
	C II] λ2326[a]	8309 ± 11	0.46 ± 0.11	1100 ± 700	25 ± 9

Notes. Column (1): source redshift, column (2): emission-line identification, column (3): observed wavelength, measured in Å, column (4): integrated flux density, measured in 10^{-16} erg s^{-1} cm^{-2}, column (5): deconvolved FWHM, measured in km s^{-1}, and column (6): rest-frame equivalent width, measured in Å.
[a]Marginal detection only.

(e.g. De Breuck et al. 2000b). An alternative possibility is that there are several different regions described by a combination of both shocks and photoionization, with the shock contribution being most significant near the radio lobes. As the size of the radio source is so small, we do not have sufficient spatial resolution to distinguish between these regions.

Assuming that the line ratios can be described by the photoionization mechanism, the hydrogen density is consistent with 100–1000 cm^{-3}, but cannot be constrained due to the degeneracy in the parameters of the photoionization models. The ultraviolet (UV) line ratios are reasonably consistent with the UV–optical diagnostic diagrams using a [O III]/Hβ $\sim$ 8 ratio (Humphrey 2004), although these diagrams are less reliable because of the possibly different apertures on the object. Moreover, if the detection of N V λ1240 is confirmed, this would imply relatively high N V/C IV ($\approx$0.76) and N V/He II ($\approx$2.1) ratios, as seen in several other $z \sim 2.5$ radio galaxies, and interpreted as evidence of supersolar metallicities (Vernet et al. 2001).

5.2 VLT/*Spitzer* imaging

Here we discuss the host galaxy properties ascertained from our VLT ISAAC and *Spitzer* IRAC images. The top left- and right-hand panels of Fig. 5 show overlays of the radio source on the ISAAC H- and K_s-band images, while the bottom left- and right-hand panels show similar overlays on the IRAC 3.6- and 8.0-μm images. Although not shown, the 4.5-μm image is very similar in appearance to the 3.6-μm image and the 5.8-μm image is of low S/N. The resolution in the 3.6- and 8.0-μm images is $\sim$1.4 and $\sim$1.7 arcsec, respectively.

The near- to mid-IR SED of PKS B0529−549 shows that the 3.6- and 4.5-μm emission is clearly dominated by an old stellar

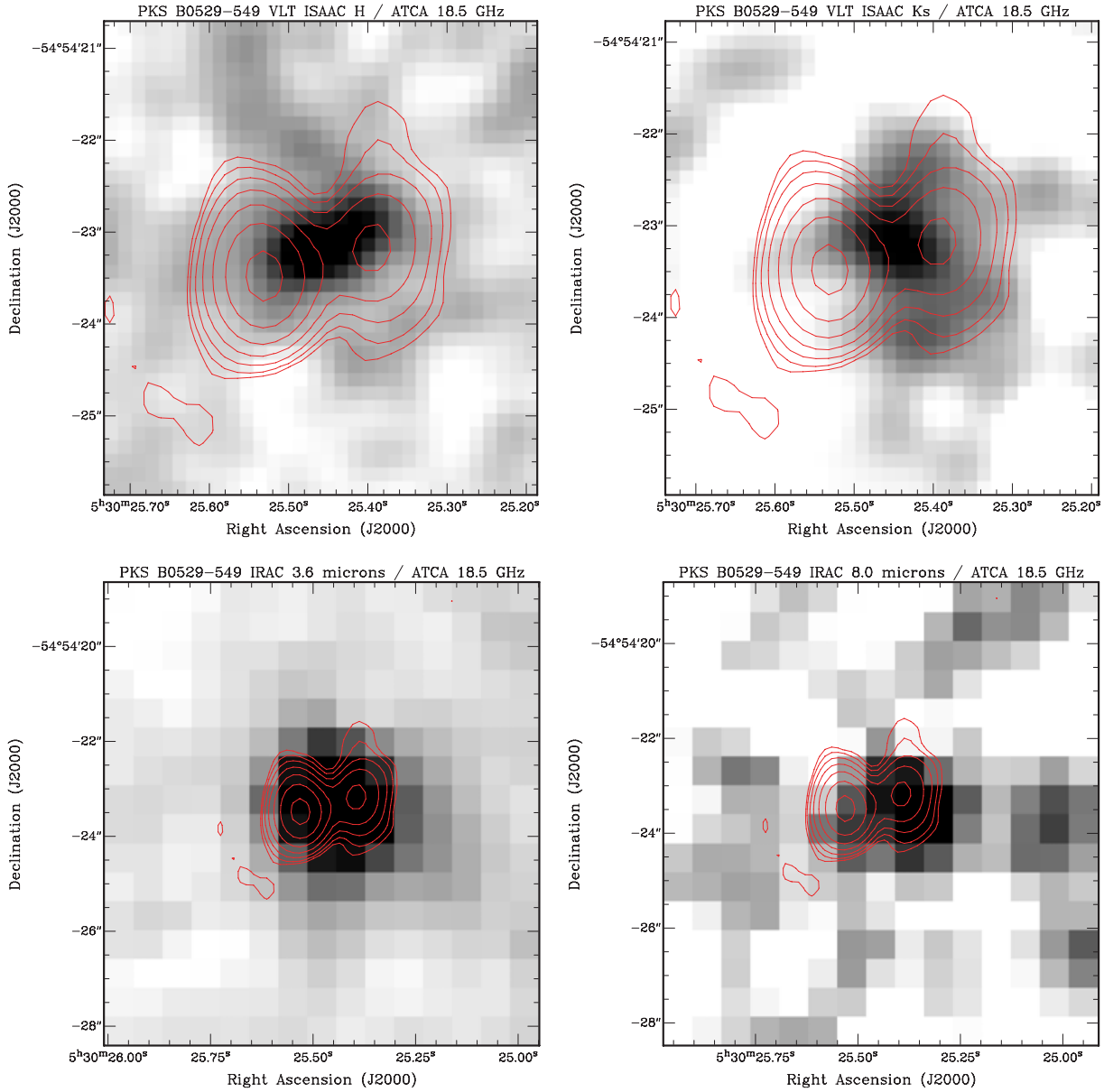

Figure 5. Smoothed ISAAC H- and K_s-band images (top left- and right-hand panels) and *Spitzer* IRAC 3.6- and 8.0-„ m images (bottom left- and right-hand panels) of PKS B0529−549, overlaid with ATCA 18 496-MHz contours. In each panel, the ATCA contour levels are 0.25, 0.5, 1, 2, 4, 8 and 16 mJy beam^{-1}.

population in the host galaxy (Seymour et al., in preparation). However, the flux in the 8-μm image is beyond the turnover of the stellar population. As the flux is higher than that in the three shorter wavelength IRAC bands, the 8-μm image must therefore be dominated by hot dust emission (Seymour et al., in preparation). The small spatial offset seen with respect to the 3.6 (and 4.5) μm emission suggests that the hot dust emission may be offset from the host galaxy. However, as the IRAC images are relatively shallow, the offset may also be due to low S/N.

The ISAAC/ATCA overlays in Fig. 5 suggest that the radio emission may extend beyond the host galaxy. We estimate that the relative radio to near-IR astrometry is accurate to ∼0.1 arcsec, which is the astrometric uncertainty of the 2MASS relative to the International Celestial Reference System (Skrutskie et al. 2006). Combining this in quadrature with the positional uncertainties in the radio and near-IR images gives an overall astrometric uncertainty of ∼0.25 arcsec. Note that we smoothed the *H*- and K_s-band images with a 0.5-arcsec FWHM Gaussian to improve the S/N. The *H*-band emission appears to be elongated along the radio axis, and is dominated by extended [O III] λλ4959,5007 emission which falls in this band. However, the K_s-band emission is not affected by emission-line contamination: the *K*-band spectrum of PKS B0529−549 (Humphrey 2004) shows only one bright emission line (Hα) which falls outside the transmission of the K_s filter used for the ISAAC imaging. The K_s-band image shows that the host galaxy is located nearer to the western radio lobe while the eastern lobe (the one with the high RM) seems to be located just outside the host galaxy (∼0.8 arcsec from the host galaxy centroid).

The K_s-band magnitude in our ISAAC image of the host galaxy is 20.0 ± 0.2 mag (1 arcsec aperture). We did not correct for Galactic extinction or airmass variations as these terms are negligible compared to the uncertainty in the photometry. The K_s-band flux falls well below an extrapolation of the old stellar population SED (Seymour et al., in preparation), implying a significant amount of extinction (∼1.6 mag) in this object and/or residual aperture correction effects. As the observed-frame K_s-band emission corresponds to rest-frame visual emission, this extinction value is consistent with the near-IR spectroscopy of Humphrey (2004), who found that the visual internal extinction value A_V may be as high as 2.6 mag in PKS B0529−549.

6 DISCUSSION

6.1 Rotation measure

The most striking result of our radio analysis of PKS B0529−549 is the huge rest-frame RM of −9600 rad m^{-2} in the eastern lobe. This RM is one of the largest observed in an extragalactic source, and as we will argue in this section, is the largest reported so far in the environment of a $z > 2$ radio galaxy. The previous largest such RM observed in a $z > 2$ radio galaxy is 6250 rad m^{-2} in the $z = 2.156$ source PKS B1138−262 (Carilli et al. 1997). In contrast, the median rest-frame RM of the $z > 2$ radio galaxies from the Carilli et al. (1997) and Pentericci et al. (2000a) studies is ∼700 rad m^{-2}. However, this median value will not be representative of the $z > 2$ radio galaxy population as a whole. As in our study, the Carilli et al. (1997) and Pentericci et al. (2000a) observations sample high rest-frame frequencies, and therefore only a restricted range of high rest-frame RMs at least several hundred rad m^{-2} in magnitude can be reliably deduced.

In determining the physical origin of the extreme RM, it is crucial to note that PKS B0529−549 is a CSS source. For comparison, PKS B1138−262 has a largest angular size of 15.8 arcsec (Carilli et al. 1997), which corresponds to a linear size of 133 kpc in our adopted cosmology. CSS sources commonly have large RMs, for example, ∼20 per cent of sources in the B3–VLA CSS sample have RMs $\geqslant 1000$ rad m^{-2} (Fanti et al. 2004). Moreover, extremely high rest-frame RMs have been observed in the high-redshift CSS quasars OQ 172 ($RM = 22\,400$ rad m^{-2}, $z = 3.535$, Kato et al. 1987; O'Dea 1998) and SDSS J1624+3758 ($RM = 18\,350$ rad m^{-2}, $z = 3.377$, Benn et al. 2005). It should be stressed that the sizes of the radio sources in these objects, and CSS sources in general, are much smaller than their host galaxies and so the Faraday screen responsible for the RM is most likely to be the magnetized interstellar environment. In fact, the extreme RM in OQ 172 has been shown to be confined to the nuclear environment (O'Dea 1998, and references therein).

Despite the fact that PKS B0529−549 is a CSS source, the magnetized ambient interstellar medium *will not* be a cause of the extreme RM if the eastern lobe is indeed located outside the host galaxy, as is suggested in the K_s-band/ATCA overlay in Fig. 5. However, we stress that the K_s-band image is very shallow, and therefore we might not be detecting low surface brightness diffuse stellar emission. Moreover, as discussed in Section 5.2, a large amount of dust may be obscuring the host galaxy. Hence, both the radio lobes of PKS B0529−549 could still be inside the host galaxy, albeit in the outer parts. We consider it unlikely that the host galaxy is significantly larger than the radio lobe separation of ∼10 kpc: near-IR imaging of radio galaxies of similar redshift to PKS B0529−549 by van Breugel et al. (1998) and Pentericci et al. (2001) reveals that the host galaxies have linear sizes up to ∼10 kpc. In addition, a dense interstellar medium producing a large RM is unlikely to be at the edge of the host galaxy. If this were in fact the case, then we may have expected the K_s-band emission to be extended towards the eastern lobe, but this is not apparent in Fig. 5.

Assuming that the RM in the eastern lobe is not being produced by the interstellar medium within the host galaxy, we now investigate two other possibilities. To test whether PKS B0529−549 resides in a cluster, we have looked for source overdensities using the *Spitzer* IRAC data, but find no evidence for this (Galametz, private communication). In addition, van der Werf, Moorwood & Bremer (2000) have searched unsuccessfully for an overdensity of Hα emitters in the field of PKS B0529−549. Although our IRAC images are relatively shallow, it thus seems unlikely that a dense protocluster environment on scales of hundreds of kpc is responsible for the large RM. However, an alternative hypothesis that a gaseous halo is responsible for the extreme RM is supported by the fact that PKS B0529−549 is known to be surrounded by a ∼45 kpc Lyα halo (van Ojik et al. 1997), as discussed in Section 5.1. Indeed, a dense halo environment is suggested by the observation that strong Lyα absorption (H I column density $= 10^{19.2}$ cm^{-2}) occurs over the spatial scale of the halo at the galaxy redshift (van Ojik et al. 1997).

Studies at low redshift find that powerful radio galaxies with substantial Faraday rotation are located in clusters composed of hot X-ray emitting gas with temperature $\sim 10^7$ K (Carilli & Taylor 2002, and references therein). These sources have been found to have RMs as large as ∼20 000 rad m^{-2}, observed in the $z = 0.464$ source 3C 295 (Perley & Taylor 1991). Carilli et al. (1997) and Pentericci et al. (2000a) speculated that the extreme RMs in their HzRG samples are also due to magnetized X-ray emitting cluster gas. Indeed, extended X-ray emission has been observed around PKS B1138−262, likely due to thermal emission from gas of density ∼0.05 cm^{-3}, though the morphology of the X-ray emission is not what would be expected from a normal cluster atmosphere (Carilli et al. 2002).

In their analysis of the Lyα emission from a sample of HzRGs, including PKS B0529−549, van Ojik et al. (1997) assumed that the radio-emitting plasma and the external hot gas in the halo are in pressure equilibrium such that $n_e T \sim 10^6$ cm^{-3} K, a typical value seen in such systems. If magnetized X-ray emitting gas of temperature $\sim 10^7$ K is causing the extreme RM in PKS B0529−549, then the electron density in this gas will be $n_e \sim 0.1$ cm^{-3}. With this rough estimate of the electron density, we can use equation (1) to estimate the magnetic field strength responsible for the RM. Letting the path length be the ∼20 kpc characteristic radius of the Lyα halo, and assuming a constant magnetic field and electron density, we find that $n_e B_\parallel \approx 0.6$, where $B_\parallel$ is the net magnetic field component along the line of sight. It follows that $B_\parallel \sim 6\,\mu$G. The magnetic field strength $B = \sqrt{3} B_\parallel$ is then $\sim 10\,\mu$G. This is consistent with the typical magnetic field strengths of ∼5–10 μG found in low-redshift clusters containing sources with extreme RMs (Carilli & Taylor 2002). However, we stress that our estimate of the magnetic field strength remains very uncertain until we can obtain X-ray observations of PKS B0529−549 to better constrain the electron density.

The expected mass M of the X-ray emitting gas inferred to be responsible for the extreme RM in PKS B0529−549 can be estimated roughly using $M \approx n_e m_p f_v V$, where m_p is the proton mass, f_v the volume filling factor and V the volume occupied by the X-ray gas. Assuming that the gas consists solely of fully ionized hydrogen contained within a sphere of radius 20 kpc, $n_e = 0.1$ cm^{-3}, and the filling factor of the hot gas is unity, then $M \sim 10^{11}$ M$_\odot$. For comparison, the estimated mass of the hot gas in PKS B1138−262 is 2.5×10^{12} M$_\odot$ (Carilli et al. 2002). Moreover, the estimated mass of the X-ray emitting gas in PKS B0529−549 is approximately three orders of magnitude higher than the mass of the Lyα emitting gas (1.4×10^8 M$_\odot$; van Ojik et al. 1997). If we assume that the X-ray emission is thermal bremsstrahlung from 10^7 K gas, then an order of magnitude estimate for the X-ray luminosity is $\sim 10^{43}$ erg s^{-1}. This estimate is similar in value to published upper limits for the extended thermal X-ray luminosity in $z > 2$ radio galaxies, which range from $\sim 4 \times 10^{43}$ to $\sim 10^{45}$ erg s^{-1} (Carilli et al. 2002; Fabian, Crawford & Iwasawa 2002; Scharf et al. 2003; Overzier et al. 2005).

6.2 Spectral energy distributions

Another piece of evidence suggesting that the large RM in the eastern lobe of PKS B0529−549 arises from a type of dense environment is that the SEDs of the individual radio components and the overall source are straight, that is, they are power law in nature (see Fig. 2). The lack of spectral steepening is intriguing, given the very high rest-frame frequencies (up to ∼70 GHz) we are sampling. Indeed, the USS selection technique for finding HzRGs is based on the correlation between z and α, which is often explained as resulting from a k-corrected concave radio spectrum that exhibits increasing energy losses at high redshift due to increased inverse Compton scattering off the cosmic microwave background (e.g. De Breuck et al. 2000a). However, Klamer et al. (2006) recently cast doubt on the significance of a k-correction. In a sample of 37 USS-selected radio galaxies, not one source shows any signs of spectral steepening at high frequencies, and 89 per cent can be described by a single power law. Given that the vast majority of USS sources in the nearby Universe are located at the centres of rich clusters, Klamer et al. (2006) postulated that the z–α correlation may result from an increased fraction of radio galaxies residing in regions of higher ambient density at high redshift. If the large RM we have measured is due to the dense environment in the Lyα halo, then the SED of PKS B0529−549 is consistent with this picture.

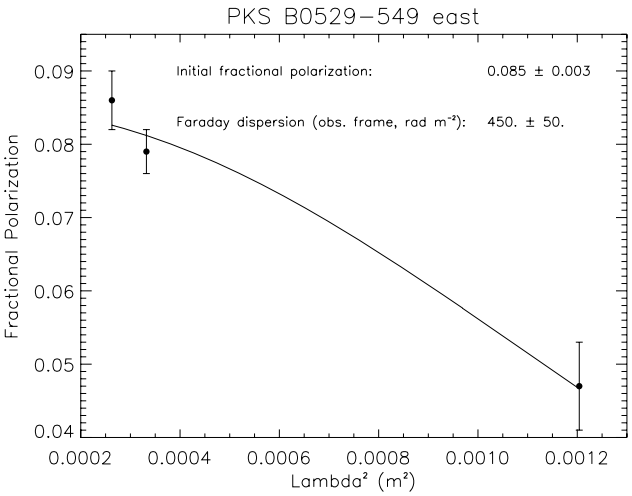

Figure 6. Fractional polarization versus λ^2 for the eastern lobe of PKS B0529−549. The solid line indicates the inverse-variance weighted fit derived from Burn's law. The initial fractional polarization and Faraday dispersion are stated in the top right-hand corner of the panel.

6.3 Faraday screen

The fractional polarization measurements discussed in Section 4.3 allow us to investigate the structure of the Faraday screen responsible for the RM in the eastern lobe. We make a standard assumption that the Faraday screen is in the foreground of the radio source, such that the thermal plasma is separate from the radio-emitting relativistic plasma. We assume further that the screen consists of cells of a given characteristic size in which the magnetic fields are coherent. Depending on the size of the telescope beam, we will measure the average RM over a given number of cells, which in turn depolarizes the source. Assuming that the RM distribution is Gaussian with dispersion σ, and that the screen is unresolved (cell size $\ll$ beam size), the fractional polarization at an observed wavelength λ is given by Burn (1966):

$$m(\lambda) = m_0 \exp(-2\sigma^2\lambda^4), \quad (8)$$

where m_0 is the fractional polarization before any depolarization occurs.

As shown in Fig. 6, the depolarization is well modelled by Burn's law (reduced $\chi^2 = 1.26$), implying that the cell size is much less than the beam size (∼6 kpc at $z = 2.575$). We find that $m_0 = 0.085 \pm 0.003$ and $\sigma = 450 \pm 50$ rad m^{-2}. In the rest-frame of PKS B0529−549, the dispersion is then $\sigma(1+z)^2 = 5800 \pm 700$ rad m^{-2}. This dispersion value implies that the rest-frame RM in the eastern lobe ranges from approximately -3800 rad m^{-2} to as high as $-15\,400$ rad m^{-2}.

The large rest-frame Faraday dispersion observed in PKS B0529−549 is consistent with the properties of the B3–VLA CSS sample (Fanti et al. 2004), in which the rest-frame Faraday dispersion (and RM) is found to increase with increasing redshift. In this sample, no sources with rest-frame Faraday dispersions >1000 rad m^{-2} are at $z < 1$. The sources with rest-frame Faraday dispersions >1000 rad m^{-2} are sufficiently depolarized such that the median fractional polarization at 1.4 GHz is only ∼0.4 per cent. We expect the eastern lobe of PKS B0529−549 to show similar behaviour.

7 CONCLUSIONS

We have drawn the following conclusions based on our study of PKS B0529−549.

(i) The eastern radio lobe of PKS B0529−549 has an extreme rest-frame RM of -9600 ± 1000 rad m^{-2}, the largest reported thus far in association with a $z > 2$ radio galaxy.

(ii) We postulate that the RM is due to $\sim 10^7$ K, dense, magnetized gas of total mass $\sim 10^{11}$ M$_\odot$ in the Lyα halo surrounding the host galaxy. We estimate the magnetic field strength of this gas to be ~ 10 μG. In addition, if the X-ray emission from this gas is thermal in origin, then we estimate the X-ray luminosity to be $\sim 10^{43}$ erg s^{-1}.

(iii) The rest-frame dispersion in the Faraday screen causing the RM is 5800 ± 700 rad m^{-2}. Thus, the RM in the eastern lobe ranges from approximately -3800 rad m^{-2} to as much as $-15\,400$ rad m^{-2}. We also find that the cell size in the Faraday screen is consistent with being much smaller than the ∼6 kpc size of the beam.

(iv) X-ray observations are needed to more accurately determine the electron density and gas mass in the Lyα halo. Furthermore, additional sensitive high-frequency radio observations would enable the RM in the western lobe to be calculated, allowing for a more detailed study of the environment in which the host galaxy is situated.

(v) Our NTT spectrum of PKS B0529−549 has allowed for more accurate emission-line properties to be deduced. We suggest that the revised line ratios are best described by a photoionization model. In addition, the N V line ratios suggest the presence of supersolar metallicities in the emission-line gas.

(vi) The K_s-band magnitude (20.0 ± 0.2 mag) and the near- to mid-IR SED imply that the host galaxy is significantly obscured by dust (internal visual extinction ∼1.6 mag). Moreover, the 8.0-μm emission is dominated by a hot dust component.

ACKNOWLEDGMENTS

JWB acknowledges the receipt of both an Australian Postgraduate Award and a Denison Merit Award. RWH acknowledges support from the Australian Research Council. We thank Bryan Gaensler, Montse Villar-Martín, Andrew Humphrey and Elaine Sadler for valuable discussions, and the anonymous referee for helpful suggestions. The ATCA is part of the Australia Telescope which is funded by the Commonwealth of Australia for operation as a National Facility managed by the CSIRO. This research has made use of the NASA/IPAC Extragalactic Database (NED) which is operated by the Jet Propulsion Laboratory, California Institute of Technology, under contract with the National Aeronautics and Space Administration (NASA). This work is based (in part) on observations made with the *Spitzer Space Telescope*, which is operated by the Jet Propulsion Laboratory, California Institute of Technology under a contract with NASA. This publication makes use of data products from the Two Micron All Sky Survey, which is a joint project of the University of Massachusetts and the Infrared Processing and Analysis Center/California Institute of Technology, funded by the NASA and the National Science Foundation.

REFERENCES

Allen M. G., Dopita M. A., Tsvetanov Z. I., 1998, ApJ, 493, 571
Athreya R. M., Kapahi V. K., McCarthy P. J., van Breugel W., 1998, A&A, 329, 809
Beasley A. J., Gordon D., Peck A. B., Petrov L., MacMillan D. S., Fomalont E. B., Ma C., 2002, ApJS, 141, 13
Benn C. R., Carballo R., Holt J., Vigotti M., González-Serrano J. I., Mack K.-H., Perley R. A., 2005, MNRAS, 360, 1455
Blumenthal G., Miley G., 1979, A&A, 80, 13
Bolton J. G., Savage A., Wright A. E., 1977, Aust. J. Phys. Astrophys. Suppl., 41, 1
Bolton J. G., Savage A., Wright A. E., 1979, Aust. J. Phys. Astrophys. Suppl., 46, 1
Bornancini C. G., Lambas D. G., De Breuck C., 2006, MNRAS, 366, 1067
Broten N. W., MacLeod J. M., Vallee J. P., 1988, Ap&SS, 141, 303
Burn B. J., 1966, MNRAS, 133, 67
Cardelli J. A., Clayton G. C., Mathis J. S., 1989, ApJ, 345, 245
Carilli C. L., Taylor G. B., 2002, ARA&A, 40, 319
Carilli C. L., Owen F. N., Harris D. E., 1994, AJ, 107, 480
Carilli C. L., Röttgering H. J. A., van Ojik R., Miley G. K., van Breugel W. J. M., 1997, ApJS, 109, 1
Carilli C. L., Harris D. E., Pentericci L., Röttgering H. J. A., Miley G. K., Kurk J. D., van Breugel W., 2002, ApJ, 567, 781
Condon J. J., 1997, PASP, 109, 166
De Breuck C., van Breugel W., Röttgering H. J. A., Miley G., 2000a, A&AS, 143, 303
De Breuck C., Röttgering H., Miley G., van Breugel W., Best P., 2000b, A&A, 362, 519
De Breuck C., van Breugel W., Stanford S. A., Röttgering H., Miley G., Stern D., 2002, AJ, 123, 637
De Breuck C. et al., 2003, A&A, 401, 911
Dekker H., Delabre B., Dodorico S., 1986, in Crawford D. L., ed., Proc. SPIE Vol. 627, Instrumentation in Astronomy VI. SPIE, Bellingham, p. 339
Eales S., Rawlings S., Law-Green D., Cotter G., Lacy M., 1997, MNRAS, 291, 593
Fabian A. C., Crawford C. S., Iwasawa K., 2002, MNRAS, 331, L57
Fanti C. et al., 2004, A&A, 427, 465
Fazio G. G. et al., 2004, ApJS, 154, 10
Gaensler B. M., Haverkorn M., Staveley-Smith L., Dickey J. M., McClure-Griffiths N. M., Dickel J. R., Wolleben M., 2005, Sci, 307, 1610
Gardner F. F., Whiteoak J. B., 1966, ARA&A, 4, 245
Garrington S. T., Leahy J. P., Conway R. G., Laing R. A., 1988, Nat, 331, 147
Greve T. R., Ivison R. J., Papadopoulos P. P., 2004, A&A, 419, 99
Hamuy M., Walker A. R., Suntzeff N. B., Gigoux P., Heathcote S. R., Phillips M. M., 1992, PASP, 104, 533
Hamuy M., Suntzeff N. B., Heathcote S. R., Walker A. R., Gigoux P., Phillips M. M., 1994, PASP, 106, 566
Humphrey A., 2004, PhD thesis, Univ. Hertfordshire
Inskip K. J., Best P. N., Longair M. S., MacKay D. J. C., 2002, MNRAS, 329, 277
Jarvis M. J., Rawlings S., Eales S., Blundell K. M., Bunker A. J., Croft S., McLure R. J., Willott C. J., 2001, MNRAS, 326, 1585
Kato T., Tabara H., Inoue M., Aizu K., 1987, Nat, 329, 223
Klamer I. J., Ekers R. D., Sadler E. M., Weiss A., Hunstead R. W., De Breuck C., 2005, ApJ, 621, L1
Klamer I. J., Ekers R. D., Bryant J. J., Hunstead R. W., Sadler E. M., De Breuck C., 2006, MNRAS, 371, 852
Kurk J. D. et al., 2000, A&A, 358, L1
Laing R. A., 1988, Nat, 331, 149
Large M. I., Mills B. Y., Little A. G., Crawford D. F., Sutton J. M., 1981, MNRAS, 194, 693
Mauch T., Murphy T., Buttery H. J., Curran J., Hunstead R. W., Piestrzynski B., Robertson J. G., Sadler E. M., 2003, MNRAS, 342, 1117
Miley G., 1980, ARA&A, 18, 165
Moorwood A. et al., 1998, The Messenger, 94, 7
Muxlow T. W. B., Garrington S. T., 1991, in Hughes P. A., ed., Beams and Jets in Astrophysics. Cambridge Univ. Press, Cambridge, p. 52
O'Dea C. P., 1998, PASP, 110, 493
Overzier R. A., Harris D. E., Carilli C. L., Pentericci L., Röttgering H. J. A., Miley G. K., 2005, A&A, 433, 87

Pentericci L., Van Reeven W., Carilli C. L., Röttgering H. J. A., Miley G. K., 2000a, A&AS, 145, 121
Pentericci L. et al., 2000b, A&A, 361, L25
Pentericci L., McCarthy P. J., Röttgering H. J. A., Miley G. K., van Breugel W. J. M., Fosbury R., 2001, ApJS, 135, 63
Perley R. A., Taylor G. B., 1991, AJ, 101, 1623
Reuland M. et al., 2003, ApJ, 592, 755
Ricci R., Prandoni I., Gruppioni C., Sault R. J., De Zotti G., 2004, A&A, 415, 549
Rocca-Volmerange B., Le Borgne D., De Breuck C., Fioc M., Moy E., 2004, A&A, 415, 931
Röttgering H. J. A., West M. J., Miley G. K., Chambers K. C., 1996, A&A, 307, 376
Röttgering H. J. A., van Ojik R., Miley G. K., Chambers K. C., van Breugel W. J. M., de Koff S., 1997, A&A, 326, 505
Sadler E. M. et al., 2006, MNRAS, 371, 898
Sault R. J., Teuben P. J., Wright M. C. H., 1995, in Shaw R. A., Payne H. E., Hayes J. J. E., eds, ASP Conf. Ser. Vol. 77, Astronomical Data Analysis Software and Systems IV. Astron. Soc. Pac., San Francisco, p. 433
Scharf C., Smail I., Ivison R., Bower R., van Breugel W., Reuland M., 2003, ApJ, 596, 105
Schlegel D. J., Finkbeiner D. P., Davis M., 1998, ApJ, 500, 525
Skrutskie M. F. et al., 2006, AJ, 131, 1163
Spergel D. N. et al., 2003, ApJS, 148, 175
Tielens A. G. G. M., Miley G. K., Willis A. G., 1979, A&AS, 35, 153
van Breugel W. J. M., Stanford S. A., Spinrad H., Stern D., Graham J. R., 1998, ApJ, 502, 614
van der Werf P. P., Moorwood A. F. M., Bremer M. N., 2000, A&A, 362, 509
van Ojik R., Röttgering H. J. A., Miley G. K., Hunstead R. W., 1997, A&A, 317, 358
Venemans B. P. et al., 2002, ApJ, 569, L11
Vernet J., Fosbury R. A. E., Villar-Martín M., Cohen M. H., Cimatti A., di Serego Alighieri S., Goodrich R. W., 2001, A&A, 366, 7
Villar-Martín M., Vernet J., di Serego Alighieri S., Fosbury R., Humphrey A., Pentericci L., 2003, MNRAS, 346, 273
Villar-Martín M. et al., 2006, MNRAS, 366, L1
Willott C. J., Rawlings S., Jarvis M. J., Blundell K. M., 2003, MNRAS, 339, 173
Wright A. E., Griffith M. R., Burke B. F., Ekers R. D., 1994, ApJS, 91, 111

This paper has been typeset from a TEX/LATEX file prepared by the author.